IET The Institution of Engineering and Technology WILEY

ORIGINAL RESEARCH PAPER

Energy recovery strategy for regenerative braking system of intelligent four-wheel independent drive electric vehicles

Liang Li[1] | **Xianyao Ping**[1] | **Jialei Shi**[2] | **Xiangyu Wang**[1] | **Xiuheng Wu**[1]

[1] State Key Laboratory of Automotive Safety and Energy, Tsinghua University, Beijing, China

[2] Department of Mechanical Engineering, University College London, London, UK

Correspondence
Xiuheng Wu, State Key Laboratory of Automotive Safety and Energy, Tsinghua University, Beijing 100084, China.
Email: wxh599@cau.edu.cn

Abstract
Regenerative braking system can recovery energy in various electric vehicles. Considering large computation load of global optimization methods, most researches adopt instantaneous or local algorithms to optimize the recuperation energy, and incline to study straight deceleration processes. However, uncertain drivers' intentions limit the potential exploration of economy improvement, and simple test conditions do not reflect the complexity of actual driving cycles. Herein, an innovative control architecture is designed for intelligent vehicles to overcome these challenges to some extent. Compared with traditional vehicles, driverless ones would eliminate drivers' interferences, and have more freedoms to optimize energy recovery, route tracking and dynamics stability. Specifically, a series regenerative braking system is designed, and then a three-level control architecture is first proposed to coordinate three performances. In the top layer, some rules with maximum recuperation energy is exploited off-line for optimising the velocity and control commands on-line. In the middle layer, local algorithm is used to track the commands and complex routes for optimal energy from a global perspective. In the bottom layer, hydraulic and regenerative toques are allocated. Tests are conducted to demonstrate the effectiveness of the design and control schemes.

1 | INTRODUCTION

Braking system would consume about 32.76% of total traction energy in New European Driving Cycle (NEDC), and this figure goes even 59.13% when it comes to crowded urban driving conditions [1]. Regenerative brake is a key technology to save energy, and reuse it for driving in various electric vehicles [2]. Different from friction brake of hydraulic system, regenerative brake performed by the electric motor as a generator transfers kinetic energy to electric energy [3]. For regenerative braking system (RBS), there are three important topics including the system design, blended brake control and energy efficiency evaluation [4].

Electric vehicles have the advantages not only of low impact to the environment, but also of allowing their motion to be controlled more easily than conventional vehicles for high agility, stability and energy efficiency [5]. Four-wheel independent drive electric vehicles equipped with four in-wheel motors can control each motor's torque and rotation speed quickly and precisely, which provides a prospect to improve vehicle dynamics and economy performances especially [6–8]. Not providing adequate braking deceleration, regenerative brake usually achieves co-existence with the friction brake. According to the coupling relationship between them, RBS could be mostly classified into series and parallel categories. Parallel RBS usually distributes target hydraulic pressure into four wheel cylinder averagely, and directly applies regenerative braking forces to the wheels without adjusting original friction braking forces. On the contrary, hydraulic pressure of each wheel cylinder in series RBS can be controlled independently and individually. Parallel RBS limits the optimization space of regenerative efficiency and braking stability [9], and series RBS has better potentials of braking energy recuperation and stability. One of challenges is that series RBS need more complex mechanisms and controls versus parallel RBS. Based on anti-lock braking system (ABS) or electric stability control system (ESC), series RBS has been designed to modulate wheel cylinder pressure during regenerative braking processes [10].
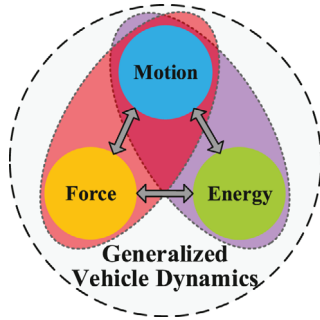
FIGURE 1 Generalised vehicle dynamics theory diagram

FIGURE 2 Case-study vehicle with designed series RBS

In regenerative braking system control field, present researches have been implemented to study the cooperation between motor and friction brakes. The most popular method to distribute braking torques of four wheels is I-curve strategy for preventing wheel lock. However, low recuperation efficiency is a fatal flaw of this strategy. To overcome this defect, hierarchical control strategies are introduced [11–14]. Upper-layer controller is to satisfy driver's intentions and dynamics stability, and lower-layer controller is designed to allocate braking torques of four wheels for maximising recuperation energy. After considering high computational loads of global optimization algorithms, hierarchical strategies usually adopt model predictive control (MPC) to achieve receding optimization and obtain local optimal solutions [15–17]. Besides hierarchical strategy, maximum-regeneration-efficiency strategy, good-pedal-feel strategy and their coordination strategy also have been proposed [18]. Meanwhile, the optimization of electric motor is also a good method to improve braking performance and regenerative energy [19]. Aforementioned literatures give priority to satisfy designated needs of drivers, and then develop braking energy recovery strategy. However, uncertainty of their behaviours increase the difficulty of prediction, and inaccurate manoeuvre of drivers would limit the energy-efficiency. How to eliminate the drivers' interferences has important significance on the vehicle performances. With the development of intelligent technologies, advanced algorithms begin to manipulate the vehicles rather than the drivers. Thus, humans' interferences in traditional vehicles could be eliminated in driverless ones to some extent.

For improving vehicle performances further, generalised vehicle dynamics theory is introduced. In generalised vehicle dynamics theory firstly proposed by our research group and shown in Figure 1, the force and energy of a vehicle are closely related with its motion. In other words, the motion has crucial effects on its dynamic stability and energy efficiency. Compared with designated velocity-tracking strategy, velocity-optimising controller in the traditional vehicles is designed for promoting further regenerative efficiency [20] without the steering angle control. Besides, two notable challenges are that braking stability on complex conditions is not considered, and optimised velocity profile and guided operation commands are difficult for drivers to be tracked accurately. But for the intelligent vehicles without the drivers, their motions co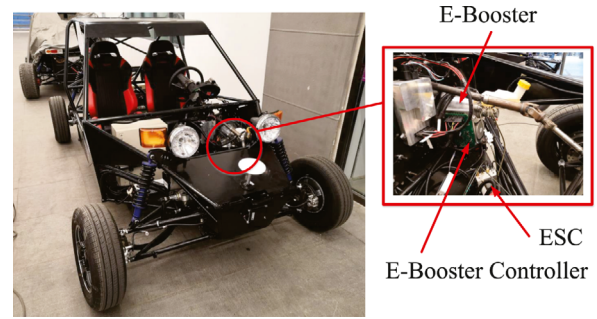uld be planned previously according to the optimization purposes, and corresponding commands are also executed better. On the basis of theoretical analysis, control algorithms would have more freedoms or space to improve recuperation energy, route tracking and dynamics stability. Thus, optimising motion could enhance regenerative efficiency, tracking error and driving stability further.

This study mainly concentrates on normal deceleration process, and ABS controller will enter the work when safety-critical driving manoeuvres [21, 22] happen. Some contributions are: firstly, a reliable series RBS based on ESC and E-booster is designed; secondly, after generalised vehicle dynamics theory is analysed, an on-line braking control strategy is proposed to coordinate recuperation energy, route tracking and dynamics stability; thirdly, some off-line data analyse and practical algorithms are combined to search optimal energy for a global perspective with appropriate computation loads. Compared with existing literatures, this study focuses on the innovative control architecture design rather than specific optimization control theory improvement.

The remainder of this article is organised as follows: a design of RBS is presented in Section 2. Section 3 gives a specific description of mathematical vehicle modelling. Section 4 proposes generalised dynamics coordination control strategy. Some controller-in-loop tests are performed in Section 5, and their results are analysed simultaneously. At the end, Section 6 draws the conclusion.

2 | SERIES REGENERATIVE BRAKING SYSTEM DESIGN

Regenerative torque of each in-wheel motor is adjusted easily by motor control unit, but independent change of each wheel cylinder's braking pressure needs reliable hydraulic structure and precise components (valves, piston pumps etc.). ESC and E-booster are developed by our research group, and has been specifically described [23, 24]. As shown in Figure 2, series RBS has been applied on four-wheel independent drive electric vehicle for recovering energy and ensuring braking safety.

As presented in Figure 3, hydraulic braking system includes mainly E-booster and ESC. Frequent modulation of hydraulic braking torque of each wheel results in the fluctuation of
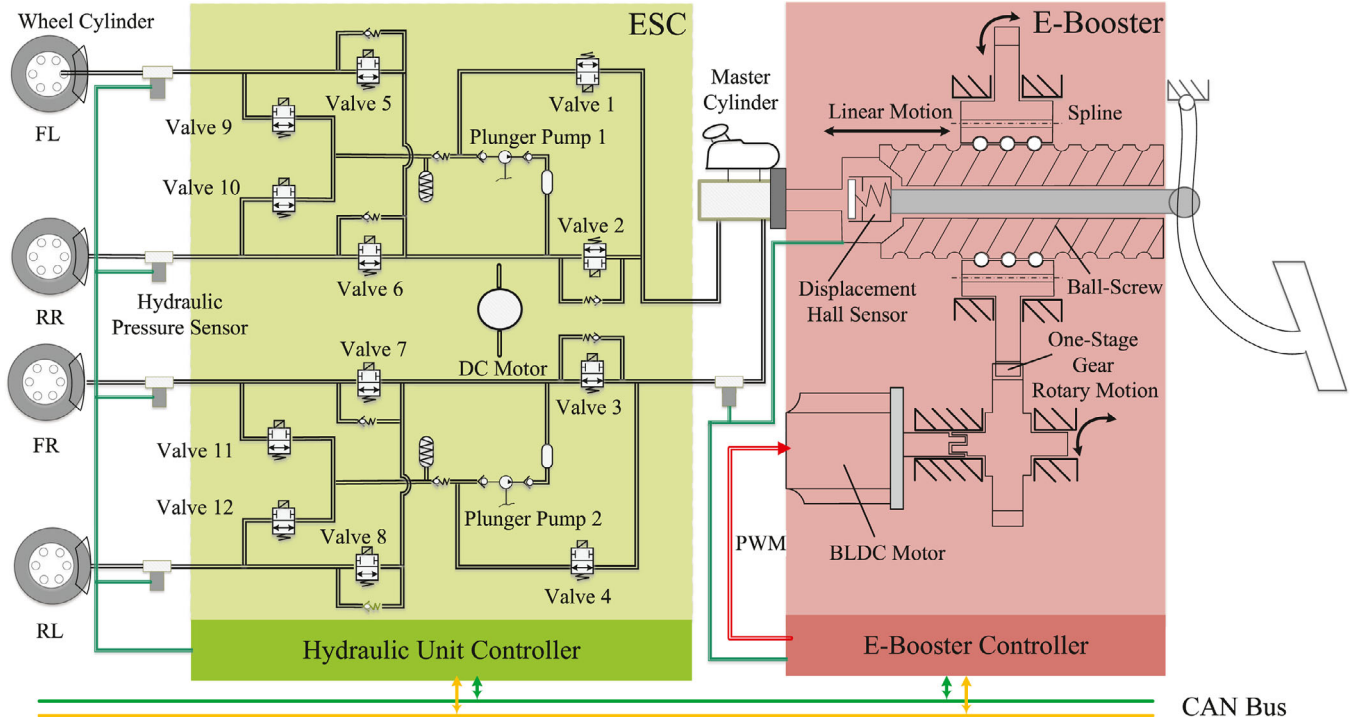
FIGURE 3 Layout of hydraulic mechanism of designed series RBS

master cylinder pressure, and worsens the brake pedal [18]. With consideration of drivers' intervenes under safety-critical circumstances, E-booster is utilised to decouple the brake pedal force with the wheel cylinder pressure. According to upper-level requestion commands, ESC would achieve designated actions accurately, such as pressure-increasing, pressure-decreasing and pressure-holding actions, to adjust each wheel cylinder pressure individually. Specifically, ESC controls the states of 12 valves and 2 piston pumps to regulate four wheel cylinder pressures. In addition, brushless direct current (BLDC) motor of E-booster also could response the upper-level commands but only modulate the master cylinder pressure.

3 | MATHEMATICAL VEHICLE MODELLING

The first step of modelling is a four-wheel vehicle dynamic body model with seven degrees of freedom. Then, numerical models of the braking system are built. This section will serve as a basis for the designs of generalised dynamics coordination control strategy.

3.1 | Body dynamics model

With consideration of the computational load and accuracy, a vehicle body dynamics model with seven degrees of freedom is introduced in this subsection. Some modelling assumptions are narrated in [25].
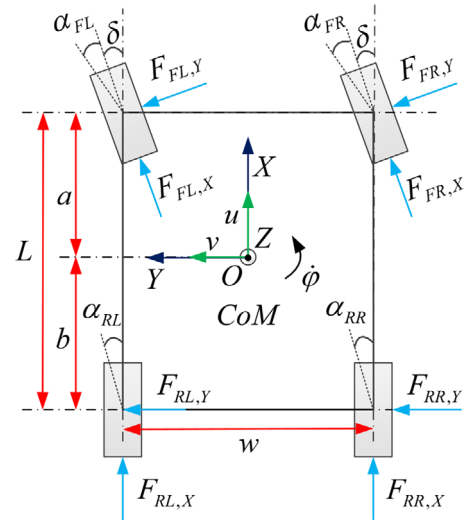

FIGURE 4 Body forces in the body-fixed reference frame

Figure 4 shows a four-wheel vehicle in the moving body-fixed coordinate system $OXYZ$ by the overview view. Several equations of longitudinal, lateral, yaw and wheel motions are given in [26].

Figure 5 presents the tire forces $F_{i,X}$, $F_{i,Y}$ and $F_{i,Z}$, $i \in \{FL, FR, RL, RR\}$ in the wheel-fixed reference frame $Wxyz$. α_i and λ_i are sideslip angle and slip ratio of the tire, respectively. For the definitions of these parameters, refer to [27, 28]. Longitudinal wheel force could be approximately replaced by the sum of regenerative and hydraulic forces. In linear region where the
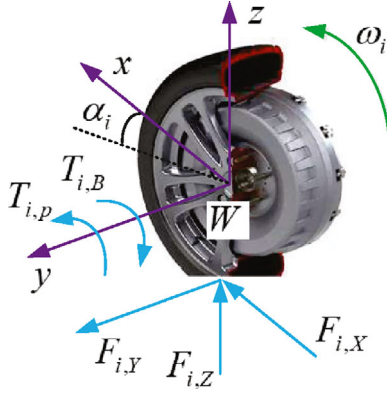
FIGURE 5 Wheel forces in the wheel-fixed reference frame

FIGURE 6 Motor efficiency map

sideslip angle of wheel is usually less than 5°, lateral wheel force is approximately proportional to its sideslip angle.

$$F_{i,Y} = -C_i \alpha_i \ (C_i > 0) \tag{1}$$

where C_i is absolute value of tyre's lateral stiffness.

3.2 | Hydraulic braking model

In series RBS, hydraulic pressure of each wheel cylinder could be adjusted individually and accurately. For the sector-shaped brake pad, its average diameter is

$$d_m = \frac{d_o + d_i}{2} \tag{2}$$

where d_o and d_i are the outer and inner diameters, respectively. Hydraulic torque of each wheel is

$$T_h = \frac{C_w \pi d_m^2 p r}{2} \tag{3}$$

where C_w, p and r are the efficiency, pressure and action radius of wheel cylinder, respectively.

3.3 | Regenerative braking model

The case-study vehicle is driven by four permanent magnet synchronous in-wheel motors, which can also work as four generators during braking procedures. It is assumed that four in-wheel motors have consistent performance, and the motor efficiency map is shown in Figure 6. The rated power and voltage for the in-wheel motor are 6 kW and 72 V, respectively.

The motor efficiency $\eta_{i,m}$ is related to the regenerative torque $T_{i,m}$ and rotation speed $n_{i,m}$, and this relationship in a non-linear form could be expressed as
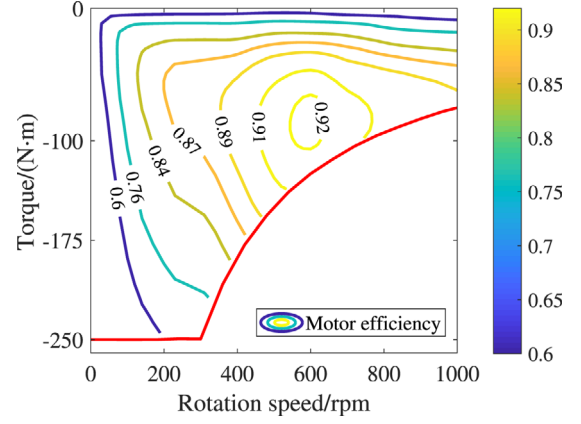
$$\eta_{i,m} = f_\eta(T_{i,m}, n_{i,m}) \tag{4}$$

Motor power $P_{i,m}$ is

$$P_{i,m} = \frac{T_{i,m} n_{i,m}}{9550} \tag{5}$$

The charge power of battery P_{bat} could be denoted as

$$P_{bat} = \eta_{bat} \sum P_{i,m} \eta_{i,m} \tag{6}$$

where η_{bat} is the battery efficiency, and its value is 0.92 for the simplification of battery model. Its rated voltage is 72 V, and the capacity is 100 A·h.

4 | GENERALISED DYNAMICS COORDINATION CONTROL

Three-level architecture of Figure 7 is first proposed to simplify the generalised coordination control problem, and decouple it into three subproblems. In the top controller, typical speed profiles with same constrains are analysed off-line by sequential quadratic programming (SQP) algorithm, and then several rules are summarised to plan optimal reference sequences of whole condition on-line. In the middle controller, MPC and linear quadratic programming regulator (LQR) are used to track the sequences and designated route, but its results are close to global solutions for recuperative energy. After braking torque of each wheel is determined, the bottom controller allocates regenerative and hydraulic torques according to the rule-based torque allocation method (RTA).

Different from instantaneous and local algorithms in tradition, generalised dynamics coordination control using local optimization converts global optimization problem into local route and command tracking problem, and is searching optimal recuperation energy. Some necessary measures, such as off-line exploration, linear approximation, and fast optimization algorithm, to balance reasonably the computation precision and load of proposed control strategy, which are significant for its real-time performance in the production vehicles. Because
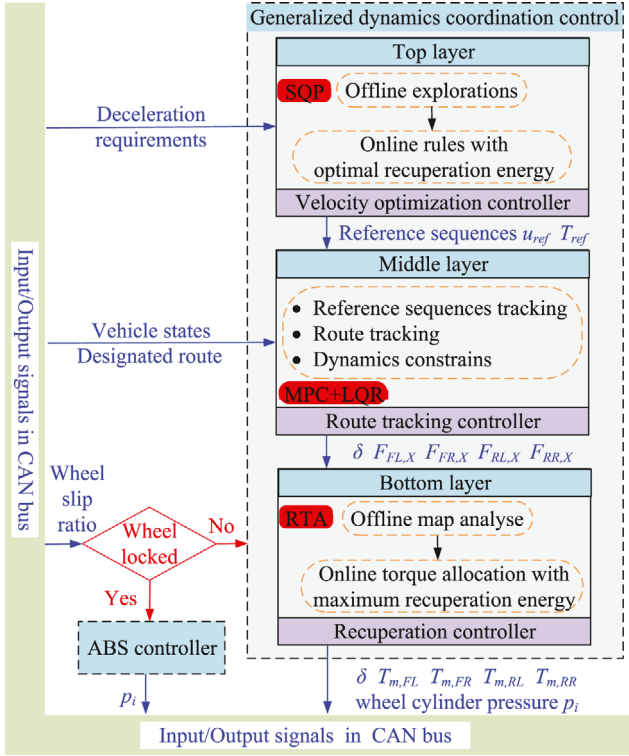
FIGURE 7 Topological structure of generalised dynamics coordination control

FIGURE 8 Optimal torque allocation factor between front and rear axles in the deceleration process
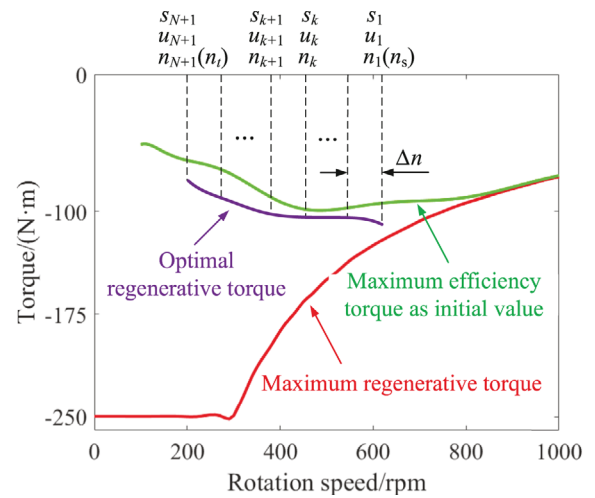
FIGURE 9 Longitudinal velocity optimization using SQP

this article mainly concentrates on normal deceleration process, the case-study vehicle is usually not with safety-critical circumstances, and the dynamics stability could be regarded as a constrain border.

4.1 | Velocity optimization controller

Under a certain deceleration, torque allocation factor ε between front and rear axles is optimised for maximum regenerative energy. The cost function of this optimization problem is Equation (7).

$$J_\varepsilon = P_{\text{bat}} \tag{7}$$

With consideration of load transfer during deceleration process, good adhesion ratio of each tire is obtained when braking torque of front axle is not less than that of rear axle. Braking torque allocation factor ξ between two axles satisfies

$$0.5 \le \xi \le 1 \tag{8}$$

The problem is solved by off-line optimization algorithm, and the results are presented in Figure 8. Within the total braking torque range of 0 to 200 N·m, each in-wheel motor has low regenerative efficiency when the total torque is distributed equally to four wheels. Thus, total braking torque provided by two in-wheel motors of front axle rather than four ones would
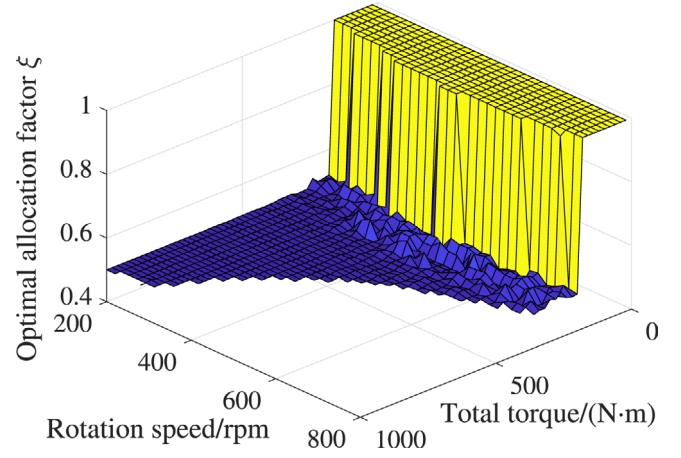
obtain higher efficiency and more regenerative energy. With the increases of deceleration intensity and total braking torque, four in-wheel motors with same output torque would work simultaneously and recover more regenerative energy. In summary, the factor is 1 when total regenerative torque is less than 200 N m. Otherwise, the factor approaches 0.5.

As for start velocity u_s and terminal velocity u_t in Figure 9, the rotation speeds of four motors are ranged from n_s and n_t with an assumption that the speeds are identical even under steering conditions. The range $[n_t, n_s]$ is divided into N finite parts equally, and average speed $n_{\text{ave},k}$ can be replaced by the mean value of n_k and n_{k+1} when N is large enough.

The system state and control variables are chosen as

$$\boldsymbol{x}_v = s \tag{9}$$

$$\boldsymbol{u}_v = [T_{m,f}, T_{m,r}]^T \tag{10}$$

where s, $T_{m,f}$ and $T_{m,r}$ are the braking distance, regenerative torques of front and rear axles, respectively. State equation is

$$\boldsymbol{x}_{v,k+1} = \boldsymbol{x}_{v,k} + \frac{Rm(u_k^2 - u_{k+1}^2)}{2(T_{m,f} + T_{m,r})} \tag{11}$$

For any interval $[u_k, u_{k+1}]$, regenerative energy $E_{v,k}$ is calculated by

$$E_{v,k} = \frac{Rmn_{\text{ave},k}\eta_{\text{bat}}(u_k - u_{k+1})}{9550} \frac{T_{m,f}\eta_{m,f} + T_{m,r}\eta_{m,r}}{T_{m,f} + T_{m,r}} \tag{12}$$

As shown in Figure 8, the breaking torque allocation factor ξ is either 0.5 or 1. In other words, $T_{m,r}$ is equal to either $T_{m,f}$ or 0. Thus,

$$E_{v,k} = \frac{Rmn_{\text{ave},k}\eta_{\text{bat}}(u_k - u_{k+1})}{9550}\eta_{m,f} \tag{13}$$

It is reasonable to choose these torques with maximum efficiency as initial values in Figure 9. Some constrains for the state and control variables are as follows

$$\begin{cases} s_t \leq \mathbf{x}_{v,N+1} \\ 2T_{\text{reg,max}} \leq T_{m,f} \leq 0 \\ 2T_{\text{reg,max}} \leq T_{m,r} \leq 0 \end{cases} \tag{14}$$

For satisfying designated travelling distance s_t, hydraulic braking is also applied to slow the vehicle down in some situations. A factor κ is defined to determine the hydraulic torque of each axle.

$$\kappa = \frac{x_{v,N+1}}{s_t} \tag{15}$$

$$T_{b,i} = (\kappa - 1)T_{m,i}, \quad i = f, r \tag{16}$$

Modified cost equation can be expressed as

$$J_v = -\sum_{i=1}^{N} E_{v,k}/\kappa \tag{17}$$

Control variables are solved by following equation

$$\boldsymbol{u}_v = \arg\min J_v \tag{18}$$

SQP algorithm suitable for non-linear system is used to solve this optimal problem, and maximum efficiency toques are regarded as initial values of SQP. Regenerative energies of some speed profiles with same start and end points are presented in Figure 10, and these profiles could reflect braking habits of different drivers to some extents. The speed profiles iii and ix are constant deceleration motions, and iv and x come from SQP optimization. The differences of reminders with time-varying
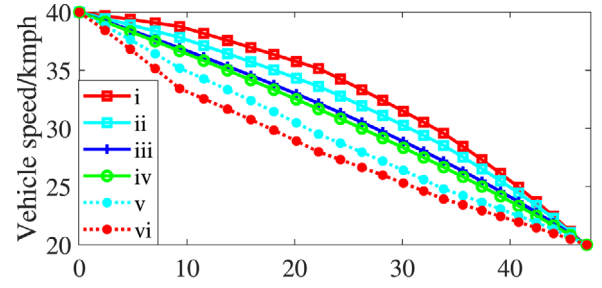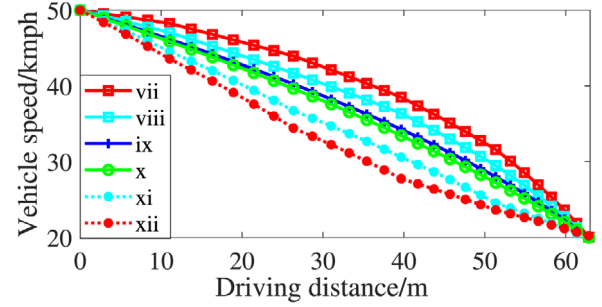
FIGURE 10 Typical speed profiles under deceleration processes
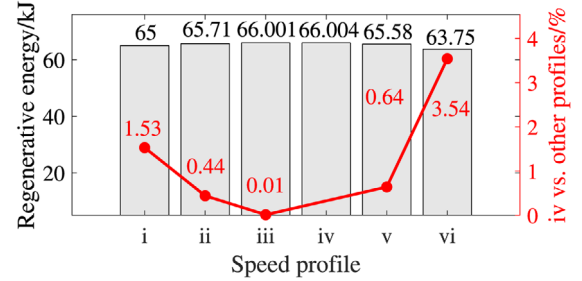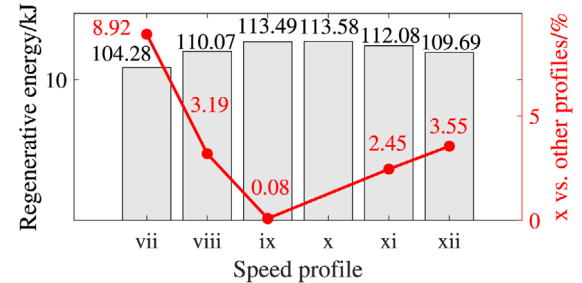
FIGURE 11 Regenerative energies and improvements without consideration of route tracking and dynamics stability

deceleration are the braking strength and strength distribution in the space.

As shown in Figure 11, speed profile has significant effect on regenerative energy, and the speed profiles iii and ix are the

closest to that of iv and x. Similar results could be also found in other deceleration processes. Given the large computation load and poor practicality of SQP in the production vehicles, a reasonable trade-off is proposed for these deceleration conditions with strict demands for the start and end points. Some rules are summarised as follows: (1) constant deceleration motion approaches optimal recuperation maximumly. (2) total regenerative torque is allocated to each wheel averagely when it is more than 200 N m; otherwise, it is allocated to the front wheels averagely. (3) the ratio of hydraulic and regenerative torques is same for every wheel.

4.2 | Route tracking controller

Without consideration of regenerative energy, optimal torque allocation sequences exist for the route tracking, which usually do not satisfy the rules of velocity optimization controller completely. Thus, it is necessary to coordinate the torques of four wheels for executing the commands from top layer and tracking complex routes well.

Compared with the constant velocity route tracking studied deeply, time-varying velocities increases the non-linearity of

where

$$
\begin{cases}
\eta_1 = F_{FL,X} - F_{FR,X} \\
\eta_2 = F_{RL,X} - F_{RR,X} \\
\eta_3 = (\xi - 1)F_{FL,X} + \xi F_{RL,X}
\end{cases}
$$

Some approximations are made as follow

$$
\cos \delta \approx 1, \ \sin \delta \approx \delta, \ \tan \delta \approx \delta \tag{22}
$$

$$
\alpha_{FL} \approx \alpha_{FR} \approx \alpha_{cf} = \frac{v + a\dot{\varphi}}{u} - \delta \tag{23}
$$

$$
\alpha_{RL} \approx \alpha_{RR} \approx \alpha_{cr} = \frac{v - b\dot{\varphi}}{u} \tag{24}
$$

So the state equation is

$$
\dot{x}_t = f_t(x_t, u_t) \tag{25}
$$

$$
f_t = \begin{bmatrix}
-u\dot{\varphi} + \dfrac{1}{m}\left(\left(F_{FL,X} + F_{FR,X}\right)\delta + 2C_{cf}\left(\delta - \dfrac{v + a\dot{\varphi}}{u}\right) + 2C_{cr}\left(\dfrac{b\dot{\varphi} - v}{u}\right)\right) \\[3mm]
v\dot{\varphi} + \dfrac{1}{m}\left(F_{FL,X} + F_{FR,X} + F_{RL,X} + F_{RR,X} - 2C_{cf}\left(\delta - \dfrac{v + a\dot{\varphi}}{u}\right)\delta \right) \\[3mm]
\dot{\varphi} \\[3mm]
\dfrac{1}{I_v}\left(2C_{cf}\left(\delta - \dfrac{v + a\dot{\varphi}}{u}\right)a - 2C_{cr}\dfrac{b\dot{\varphi} - v}{u}b + \left(F_{FL,X} + F_{FR,X}\right)a\delta + \left(F_{FR,X} + F_{RR,X} - F_{FL,X} - F_{RL,X}\right)\dfrac{w}{2}\right) \\[3mm]
u\sin\varphi + v\cos\varphi \\[1mm]
u\cos\varphi - v\sin\varphi
\end{bmatrix}
$$

control algorithm. On the one hand, simplifying mathematical models could reduce computational loads. On the other hand, it maybe also decrease control precision to some extent. For relieving above challenges, linear approximation method, MPC and LQR are adopted.

In the prediction part of MPC, system state, control and output variables of the middle controller are

$$
\mathbf{x} = [v, u, \varphi, \dot{\varphi}, Y, X]^T \tag{19}
$$

$$
\mathbf{u} = [\delta, F_{FL,X}, F_{FR,X}, F_{RL,X}, F_{RR,X}]^T \tag{20}
$$

$$
\boldsymbol{\eta} = [u, \varphi, Y, X, \eta_1, \eta_2, \eta_3]^T \tag{21}
$$

In order to track route accurately with designated start, end and their velocities, control system need to be converted from time to spatial domain.

$$
\frac{d\mathbf{x}}{ds} = \frac{d\mathbf{x}}{dt} \cdot \frac{dt}{ds} = \frac{d\mathbf{x}}{dt} \cdot \frac{1}{u} \tag{26}
$$

$$
\dot{\mathbf{x}}_s = f_s(\mathbf{x}_s, \mathbf{u}_s) = \frac{f_t}{u} \tag{27}
$$

Corresponding system output equation in spatial domain is

$$
\boldsymbol{\eta}_s = \mathbf{C}\mathbf{x}_s + \mathbf{D}\mathbf{u}_s \tag{28}
$$

where

$$C = \begin{bmatrix} 0 & 1 & 0 & 0 & 0 & 0 \\ 0 & 0 & 1 & 0 & 0 & 0 \\ 0 & 0 & 0 & 0 & 1 & 0 \\ 0 & 0 & 0 & 0 & 0 & 1 \\ 0 & 0 & 0 & 0 & 0 & 0 \\ 0 & 0 & 0 & 0 & 0 & 0 \\ 0 & 0 & 0 & 0 & 0 & 0 \end{bmatrix}, D = \begin{bmatrix} 0 & 0 & 0 & 0 & 0 \\ 0 & 0 & 0 & 0 & 0 \\ 0 & 0 & 0 & 0 & 0 \\ 0 & 0 & 0 & 0 & 0 \\ 0 & 1 & -1 & 0 & 0 \\ 0 & 0 & 0 & 1 & -1 \\ 0 & \xi-1 & 0 & \xi & 0 \end{bmatrix}$$

After necessary linearisation, the system state equation is

$$\dot{\boldsymbol{x}}_{s,k} = \boldsymbol{A}_k \boldsymbol{x}_{s,k} + \boldsymbol{B}_k \boldsymbol{u}_{s,k} + \boldsymbol{d}_{s,k} \qquad (29)$$

where

$$\boldsymbol{A}_k = \left.\frac{\partial f_s}{\partial \boldsymbol{x}_s}\right|_{\boldsymbol{x}_{s,k},\boldsymbol{u}_{s,k}}, \boldsymbol{B}_k = \left.\frac{\partial f_s}{\partial \boldsymbol{u}_s}\right|_{\boldsymbol{x}_{s,k},\boldsymbol{u}_{s,k}}$$

Discrete state equation is

$$\boldsymbol{x}_{s,k+1} = \bar{\boldsymbol{A}}_k \boldsymbol{x}_{s,k} + \bar{\boldsymbol{B}}_k \boldsymbol{u}_{s,k} + \bar{\boldsymbol{d}}_{s,k} \qquad (30)$$

where

$$\bar{\boldsymbol{A}}_k = \boldsymbol{I}_{N_x \times N_x} + \Delta S \boldsymbol{A}_k \qquad (31)$$

$$\bar{\boldsymbol{B}}_k = \Delta S \boldsymbol{B}_k \qquad (32)$$

$$\bar{\boldsymbol{d}}_{s,k} = \boldsymbol{x}_{s,k+1}^p - \bar{\boldsymbol{A}}_k \boldsymbol{x}_{s,k} - \bar{\boldsymbol{B}}_k \boldsymbol{u}_{s,k}$$

ΔS is chosen as 0.5 meters. New state variables are selected:

$$\hat{\boldsymbol{x}}_{s,k} = [\boldsymbol{x}_{s,k}, \boldsymbol{u}_{s,k-1}]^T \qquad (33)$$

$$\Delta \boldsymbol{u}_{s,k} = \boldsymbol{u}_{s,k} - \boldsymbol{u}_{s,k-1} \qquad (34)$$

Then, the state and output equations are also converted into

$$\hat{\boldsymbol{x}}_{s,k+1} = \hat{\boldsymbol{A}}_k \hat{\boldsymbol{x}}_{s,k} + \hat{\boldsymbol{B}}_k \Delta \boldsymbol{u}_{s,k} + \hat{\boldsymbol{d}}_s \qquad (35)$$

$$\hat{\boldsymbol{\eta}}_{s,k} = \hat{\boldsymbol{C}} \hat{\boldsymbol{x}}_{s,k} \qquad (36)$$

where

$$\hat{\boldsymbol{A}}_k = \begin{bmatrix} \bar{\boldsymbol{A}}_k & \bar{\boldsymbol{B}}_k \\ \boldsymbol{0}_{N_u \times N_x} & \boldsymbol{I}_{N_u \times N_u} \end{bmatrix}, \hat{\boldsymbol{B}}_k = \begin{bmatrix} \bar{\boldsymbol{B}}_k \\ \boldsymbol{I}_{N_u \times N_u} \end{bmatrix}$$

$$\hat{\boldsymbol{C}} = \begin{bmatrix} \boldsymbol{C} & \boldsymbol{0} \\ \boldsymbol{0} & \boldsymbol{D} \end{bmatrix}, \hat{\boldsymbol{d}}_s = \begin{bmatrix} \bar{\boldsymbol{d}}_{s,k} \\ \boldsymbol{0}_{N_u \times N_u} \end{bmatrix}$$

The system outputs are expressed in the form of matrices.

$$\hat{\boldsymbol{Y}} = \boldsymbol{\psi}_k \hat{\boldsymbol{x}}_{s,k} + \boldsymbol{\Theta}_k \Delta \boldsymbol{U}_k + \boldsymbol{\Gamma}_k \boldsymbol{\phi}_k \qquad (37)$$

where

$$\hat{\boldsymbol{Y}} = \begin{bmatrix} \hat{\boldsymbol{\eta}}_{s,k+1|k} \\ \hat{\boldsymbol{\eta}}_{s,k+2|k} \\ \vdots \\ \hat{\boldsymbol{\eta}}_{s,k+N_p|k} \end{bmatrix}, \boldsymbol{\psi}_k = \begin{bmatrix} \hat{\boldsymbol{C}}\hat{\boldsymbol{A}}_k \\ \hat{\boldsymbol{C}}\hat{\boldsymbol{A}}_k^2 \\ \vdots \\ \hat{\boldsymbol{C}}\hat{\boldsymbol{A}}_k^{N_p} \end{bmatrix}, \Delta \boldsymbol{U}_k = \begin{bmatrix} \Delta \boldsymbol{u}_{s,k+1|k} \\ \Delta \boldsymbol{u}_{s,k+2|k} \\ \vdots \\ \Delta \boldsymbol{u}_{s,k+N_c|k} \end{bmatrix}$$

$$\boldsymbol{\Theta}_k = \begin{bmatrix} \hat{\boldsymbol{C}}\hat{\boldsymbol{B}}_k & \boldsymbol{0} & \cdots & \boldsymbol{0} \\ \hat{\boldsymbol{C}}\hat{\boldsymbol{A}}_k\hat{\boldsymbol{B}}_k & \hat{\boldsymbol{C}}\hat{\boldsymbol{B}}_k & \cdots & \boldsymbol{0} \\ \vdots & \vdots & \ddots & \vdots \\ \hat{\boldsymbol{C}}\hat{\boldsymbol{A}}_k^{N_p-1}\hat{\boldsymbol{B}}_k & \hat{\boldsymbol{C}}\hat{\boldsymbol{A}}_k^{N_p-2}\hat{\boldsymbol{B}}_k & \cdots & \hat{\boldsymbol{C}}\hat{\boldsymbol{A}}_k^{N_p-N_c-1}\hat{\boldsymbol{B}}_k \end{bmatrix}$$

$$\boldsymbol{\Gamma}_k = \begin{bmatrix} \hat{\boldsymbol{C}} & \boldsymbol{0} & \cdots & \boldsymbol{0} \\ \hat{\boldsymbol{C}}\hat{\boldsymbol{A}}_k & \hat{\boldsymbol{C}} & \cdots & \boldsymbol{0} \\ \vdots & \vdots & \ddots & \vdots \\ \hat{\boldsymbol{C}}\hat{\boldsymbol{A}}_k^{N_p-1} & \hat{\boldsymbol{C}}\hat{\boldsymbol{A}}_k^{N_p-2} & \cdots & \hat{\boldsymbol{C}} \end{bmatrix}, \boldsymbol{\phi}_k = \begin{bmatrix} \hat{\boldsymbol{d}}_{s,k} \\ \hat{\boldsymbol{d}}_{s,k+1} \\ \vdots \\ \hat{\boldsymbol{d}}_{s,k+N_p-1} \end{bmatrix}$$

$N_p = 11$ and $N_c = 8$ are predictive and control scopes after some simulations, respectively.

In the optimization part of MPC, the cost function is expressed as following quadratic form [11]:

$$J_t = \sum_{i=1}^{N_p} \left\| \hat{\boldsymbol{\eta}}_{s,k+i|k} - \boldsymbol{\eta}_{ref,k+i|k} \right\|_Q^2 + \sum_{i=1}^{N_c} \left\| \Delta \boldsymbol{U}_{k+i|k} \right\|_R^2 + \rho \varepsilon^2 \qquad (38)$$

where η_{ref} is the desired system output, ρ is a weight factor, and ε is a relaxation factor. After some calibrations, ρ is 1000, and ε is 10.

$$\boldsymbol{Q} = \text{diag}(1000, 1000, 1000, 30, 10, 10, 10)$$

$$\boldsymbol{R} = \text{diag}(10, 0.01, 0.01, 0.01, 0.01)$$

Standard quadratic form function is

$$J_t = \begin{bmatrix} \Delta \boldsymbol{U}_k \\ \varepsilon \end{bmatrix}^T \boldsymbol{H}_k \begin{bmatrix} \Delta \boldsymbol{U}_k \\ \varepsilon \end{bmatrix} + \boldsymbol{G}_k \begin{bmatrix} \Delta \boldsymbol{U}_k \\ \varepsilon \end{bmatrix} + \boldsymbol{E}_k^T \boldsymbol{Q} \boldsymbol{E}_k \qquad (39)$$

where

$$\boldsymbol{E}_k = \boldsymbol{\psi}_k \hat{\boldsymbol{x}}_{s,k} + \boldsymbol{\Gamma}_k \boldsymbol{\phi}_k - \boldsymbol{Y}_{ref}$$

$$\boldsymbol{H}_k = \begin{bmatrix} \boldsymbol{\Theta}_k^T \boldsymbol{Q} \boldsymbol{\Theta}_k + \boldsymbol{R} & \boldsymbol{0} \\ \boldsymbol{0} & \rho \end{bmatrix}, \boldsymbol{G}_k = \begin{bmatrix} 2\boldsymbol{E}_k^T \boldsymbol{Q} \boldsymbol{\Theta}_k & \boldsymbol{0} \end{bmatrix}$$

Because there is no non-linear constrain, LQR with fast computation rate [29] is adopted to solve this problem.

$$\Delta \boldsymbol{U}_k^* = \arg\min J_t \qquad (40)$$

Necessary constrains for system control and output variables are

$$\begin{cases} \Delta U_{\min} \leq \Delta U_k \leq \Delta U_{\max} \\ U_{\min} \leq A_U \Delta U_k + U_k \leq U_{\max} \\ Y_{\min} \leq \psi_k \hat{x}_{s,k} + \Theta_k \Delta U_k + \Gamma_k \phi_k \leq Y_{\max} \end{cases} \quad (41)$$

where

$$U_k = \mathbf{1}_{N_c} \otimes u_{k-1}$$

$$A_U = \begin{bmatrix} 1 & 0 & \cdots & \cdots & 0 \\ 1 & 1 & 0 & \cdots & 0 \\ 1 & 1 & 1 & \ddots & 0 \\ \vdots & \vdots & \vdots & \ddots & \vdots \\ 1 & 1 & \cdots & 1 & 1 \end{bmatrix} \otimes I_m$$

$$\underbrace{\qquad\qquad\qquad}_{N_c \times N_c}$$

Equation 1 is established when the sideslip angle of a wheel is less than 5°. It is necessary to constrain the sideslip angle of four wheels. It is noteworthy that the angle has strong non-linear relationship with state and control variables. Although linear approximation method could be used to solve the problem, constrain precision decreases and computation load from a global perspective increases.

Sideslip angle of rear axle is usually small, and sometimes could be neglected for the simplification in engineering. As for the wheels' sideslip angle constrains in normal deceleration conditions, it is assumed that only front axle is considered, and the rear axle is neglected. Lateral acceleration of the case-study vehicle is measured easily and has linear relationship with the sideslip angle of front axle in the assumption. Therefore, the front wheels' sideslip angle constrains are equivalent to the lateral acceleration constrain. For ensuring safety and dynamic stability, body's sideslip angle and lateral acceleration are constrained by the following equations.

$$\begin{cases} \beta_{\min} \leq \beta \leq \beta_{\max} \\ a_{y,\min} \leq a_y \leq a_{y,\max} \end{cases} \quad (42)$$

4.3 | Recuperation controller

As discussed in the route tracking controller, braking torque of each wheel has been determined. For maximising recuperation energy, the in-wheel motors are prioritised to slow down the vehicle versus hydraulic wheel cylinders. Moreover, in-wheel motors have faster torque response time. Regenerative and hydraulic torques of each wheel are allocated according to the following RTA rules.

$$T_{m,i} = \begin{cases} T_{\mathrm{reg,max}} & , T_{i,X} \leq T_{\mathrm{reg,max}} < 0 \\ T_{i,X} & , T_{\mathrm{reg,max}} < T_{i,X} \leq 0 \end{cases} \quad (43)$$
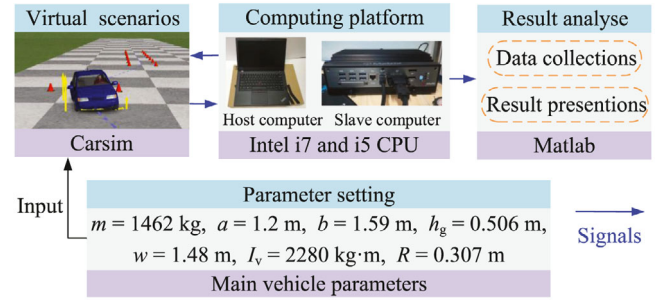

FIGURE 12 Controller-in-loop test diagram

TABLE 1 Control method comparisons between ix-T and other profiles

| Profile | Layer | | |
	Top layer	Middle layer	Bottom layer
vii	—	MPC + LQR	RTA
viii	—	MPC + LQR	RTA
ix-I	SQP	I-curve rule	RTA
ix-T	SQP	MPC + LQR	RTA
xi	—	MPC + LQR	RTA
xii	—	MPC + LQR	RTA

aAbbreviations: LQR, linear quadratic programming regulator; MPC, model predictive control; RTA, rule-based torque allocation; SQP, sequential quadratic programming.

$$T_{h,i} = F_{i,X} R - T_{m,i} \quad (44)$$

5 | CONTROLLER-IN-LOOP TEST

In Figure 12, some controller-in-loop tests are performed to verify proposed control strategy. Popular dynamics simulation software Carsim provides virtual scenarios, and the generalised dynamics coordination controllers are synthesised into a computing platform. Corner and double line change conditions are chosen to test proposed coordination control strategy. The start and end speeds are 50 and 20 km/h, respectively. The deceleration distance is about 63 meters, and the road friction coefficient is 0.75.

Typical deceleration speed profiles vii, viii, xi and xii have been discussed in the subsection 4.1, and are chosen as the control groups to reflect different driving habits of drivers to some extent. Meanwhile, hierarchical schemes and I-curve methods introduced in the Introduction would be also compared with the three-level architecture strategy. As shown in Table 1, the profiles vii, viii, xi and xii are accomplished by a hierarchical architecture, in which the middle-level controller using MPC and LQR tracks designated route, and the bottom-level one using RTA allocates regenerative and hydraulic torques to maximize recuperation energy. ix-I and ix-T profiles are achieved by the three-level architecture strategy, and their middle layers are
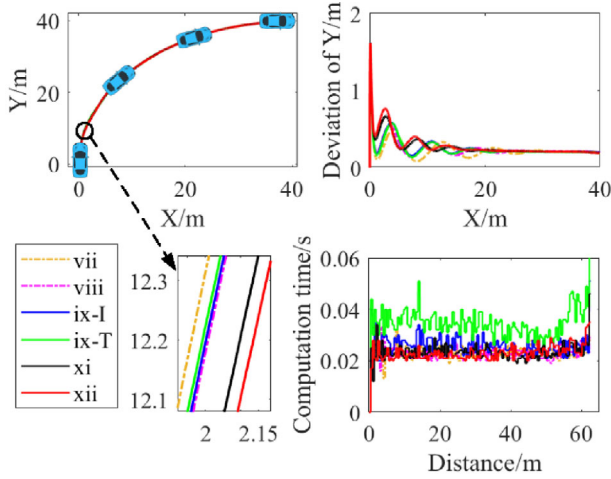
FIGURE 13 Route tracking and computation time in CC

FIGURE 14 Regenerative torque of each wheel in CC

I-curve rule and MPC+LQR, respectively. I-curve can be solved by the method of [24].

5.1 | Corner condition

Corner condition (CC) is one of typical and common driving cycles, and could be used to test the cooperative control performance between braking and steering operations. The route tracking results and computation time in corner condition are shown in Figure 13. At initial stage of the deceleration process, the vehicle speed is higher, and the fluctuation of deviation is larger versus later stages. Finally, the deviations of six speed profiles stabilize within 0.2 meters. Because it tracks designated route accurately, the case-study vehicle is regarded to be running safely.

In Figure 13, the time frequency of an algorithm is measured in terms of the computation time on the same processor. The computation time of each profile is less than 45 ms, and several sudden changes are caused by unstable performance of the computing platform. Proposed ix-T has larger computation load, and spends more 10 ms than other groups. Computation loads of six groups are suitable to the production vehicles.

Regenerative and hydraulic torques of each wheel in corner condition are presented in Figures 14 and 15, respectively. For speed profiles vii, viii, ix-T, xi and xii, total braking torque is allocated to four wheels averagely. In the speed profile ix-I, total braking toque is distributed to four wheels according to I-curve. The differences of six groups are vehicle speed profile and torque allocation strategy.

In Figure 15, large decelerations exist in the speed profiles xi and xii, and regenerative torques of four in-wheel motors cannot satisfy the braking demands. Meanwhile, the intervention of hydraulic wheel cylinders starts to increase total braking strength. Different from previous analyse, four motors are able to slow down the vehicle in speed profiles vii, viii and ix-T, and there is no intervention of the cylinders. In ix-I with I-curve strategy, larger braking torque is allocated to the front axle
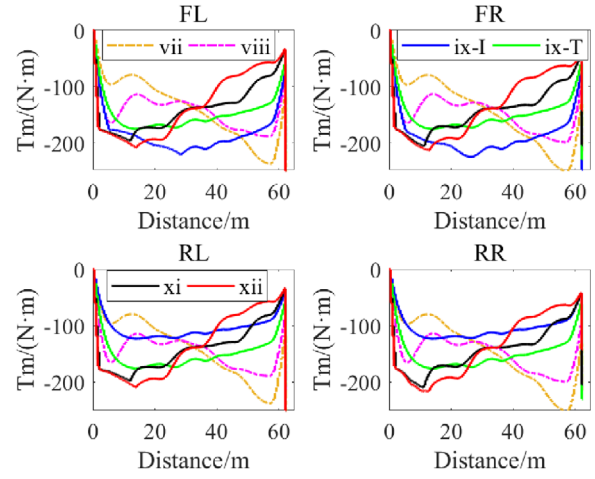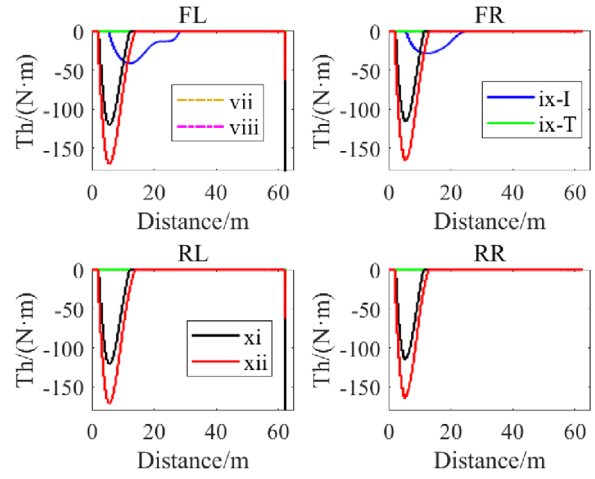

FIGURE 15 Hydraulic torque of each wheel in CC

rather than rear one for deceleration safety, and two motors of front axle need to corporate with hydraulic wheel cylinders for designated torques.

Regenerative energies of six groups are presented in Figure 16. Compared with other five groups, ix-T with three-level architecture can improve regenerative energy by 8.47%, 1.91%, 5.50%, 5.61% and 12.04%, respectively. Different from the results of Figure 11, that of Figure 16 are obtained after route, energy and safety are considered comprehensively.
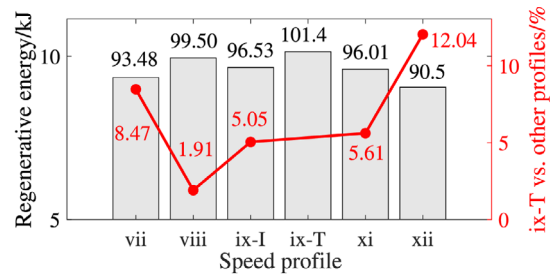

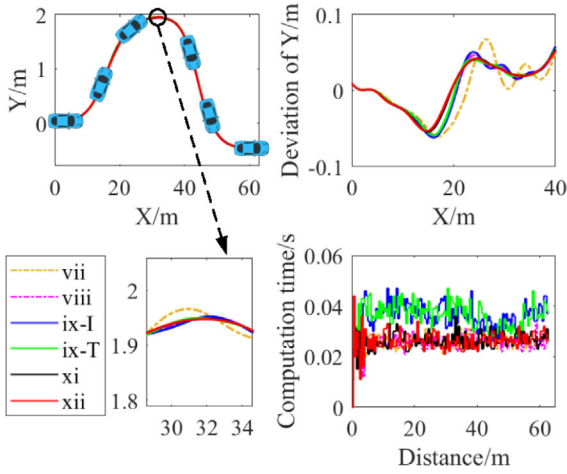**FIGURE 16** Regenerative energies of six groups in CC

FIGURE 17 Route tracking and computation time in DLCC

FIGURE 18 Regenerative torque of each wheel in DLCC

After the results of ix-T, vii, viii, xi, and xii are compared and analysed, optimal velocity and control sequences exist for maximum recuperation energy for those deceleration conditions with the start and end constrains. Tracking either designated profiles or drivers' demands has limited regenerative efficiency. According to the regenerative energy of ix-I and ix-T, the combination of MPC and LQR as a local optimization method has higher recuperation efficiency than I-curve. The differences of Figures 11b and 16 also reveal that the study about effects of velocity profile on regenerative energy could deviate the truth to some extent, and does not reflect actual regenerative energy.

5.2 | Double line change condition

Double line change condition (DLCC) is used to test route tracking and dynamics stability performances. In order to verify the effectiveness of proposed three-level architecture control strategy further, DLCC is also chosen as another test condition. The controller-in-loop results in DLCC are shown in Figures 17–20.

Similar analysis methods of CC are also applied to DLCC. Compared with other five groups, ix-T with three-level architecture can improve regenerative energy by 6.81%, 1.36%, 5.40%, 6.53% and 13.50%, respectively. The results from Figures 11b, 16 and 20 reveal that braking conditions have important impacts on recuperation energy. In other words, speed profile, route, and vehicle dynamics should be considered when the improvement methods of regenerative energy are explored. It follows that comprehensive coordination control and analyse between three performances are essential for practical application of RBS control strategy.

6 | CONCLUSION

A series regenerative braking system is designed, and a generalised coordination strategy with three-level architecture is first proposed to coordinate recuperation energy, route tracking and
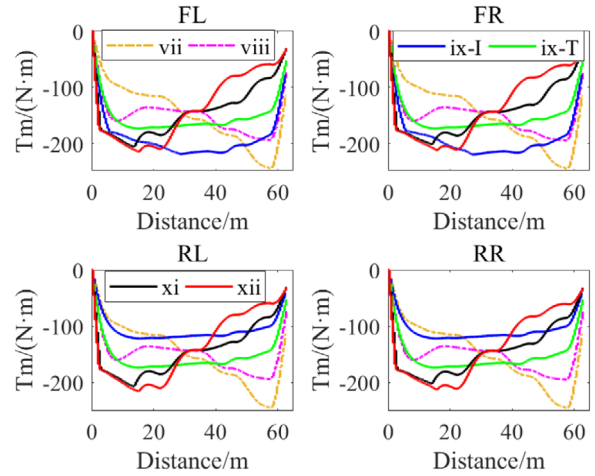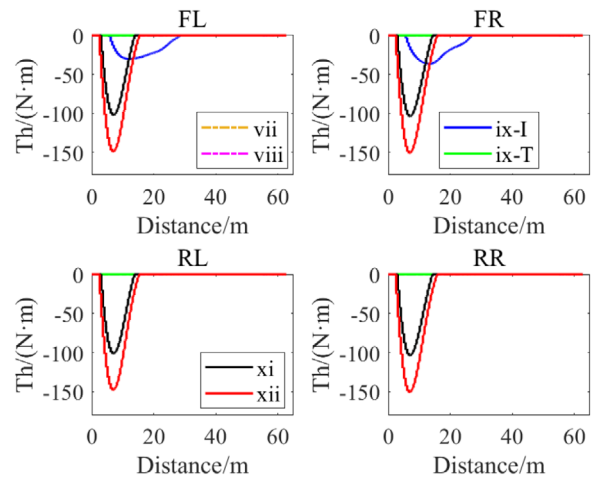

FIGURE 19 Hydraulic torque of each wheel in DLCC

dynamics stability. The controller-in-loop results demonstrate that the proposed strategy could recovery braking energy maximumly, in while complex route tracking and dynamics stability are also guaranteed effectively on corner and double line change conditions. Compared with popular I-curve and hierarchical control methods, the proposed strategy performs better without increasing computation load obviously, and has some potentials to be applied on the production vehicles.
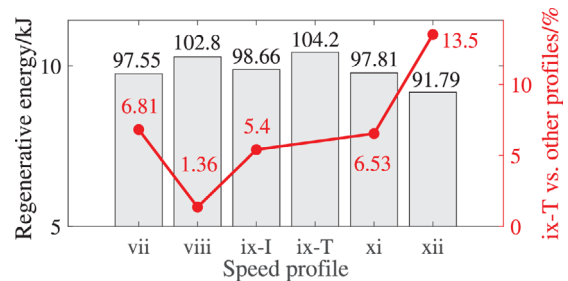

FIGURE 20 Regenerative energies of six groups in DLCC

7 | PROSPECT

It is a pity that authors could not go back to the laboratory during COVID-19, and some experiments would not to be conducted on the case-study vehicle. In the future, authors will continue to implement the experiments, and verify the effectiveness of proposed strategies. Besides, authors will also study the generalised control strategy under the emergency deceleration conditions.

NOTATION

m	vehicle mass
g	gravity acceleration
I_v	rotational inertia of the body about z-axis
I_w	rotational inertia of a wheel about y-axis
u	longitudinal velocity of CoM
v	lateral velocity of CoM
φ	yaw angle of the vehicle
a_x	longitudinal acceleration of the vehicle
a_y	lateral acceleration of the vehicle
β	sideslip angle of the vehicle body
δ	steering angle of the front wheels
w	wheel track width
a	distance from CoM to the front axle
b	distance from CoM to the rear axle
L	distance between front and rear axles
R	rolling radius of four wheels
subscript FL	front left wheel
subscript FR	front right wheel
subscript RL	rear left wheel
subscript RR	rear right wheel
$F_{i,X}$	longitudinal tire force of a tire
$F_{i,Y}$	lateral tire force of a tire
$F_{i,Z}$	vertical tire force of a tire
$T_{i,P}$	Propulsive torque of a wheel
$T_{i,B}$	Braking torque of a wheel
λ_i	slip ratio of a tire
α_i	sideslip angle of a tire
ω_i	rotational velocity of a wheel
CC	corner condition
DLCC	double line change condition

ORCID
Liang Li https://orcid.org/0000-0002-1577-408X

REFERENCES

1. Zhang, X., et al.: Energy-efficient toque allocation design of traction and regenerative braking for distributed drive electric vehicles. IEEE Trans. Veh. Technol. 67(1), 285–295 (2018)
2. Zhang, J., et al.: Time-varying delays compensation algorithm for powertrain active damping of an electrified vehicle equipped with an axle motor during regenerative braking. Mech. Syst. Sig. Process. 87, 45–63 (2017)
3. Zhang, J., et al.: Braking energy regeneration control of a fuel cell hybrid electric bus. Energy Convers. Manage. 76, 1117–1124 (2013)
4. Qiu, C., Wang, G.: New evaluation methodology of regenerative braking contribution to energy efficiency improvement of electric vehicles. Energy Convers. Manage. 119, 389–398 (2016)
5. Suzuki, Y., et al.: A study on tyre force distribution conrols for full drive-by-wire electric vehicle. Veh. Syst. Dyn. 52(sup1), 235–250 (2014)
6. Chen, G.Y., et al.: Comprehensive chassis control strategy of FWIC-EV based on sliding mode control. IET Intel. Transport Syst. 13(4), 703–713 (2019)
7. Lin, C., et al.: A multi-objective optimal torque distribution strategy for four in-wheel-motor drive electric vehicles. IEEE Access 7, 64627–64640 (2019)
8. Chatzikomis, C., et al.: An energy-efficient torque-vectoring algorithm for electric vehicles with multiple motors. Mech. Syst. Sig. Process. 128, 655–673 (2019)
9. Xu, W., et al.: Torque optimization control for electric vehicles with four in-wheel motors equipped with regenerative braking system. Mechatronics 57, 95–108 (2019)
10. Zhang, J.Z., et al.: New regenerative braking control strategy for rear-driven electrified minivans. Energy Convers. Manage. 82, 135–145 (2014)
11. Peng, H., et al.: Torque coordinated control of four in-wheel motor independent-drive vehicles with consideration of the safety and economy. IEEE Trans. Veh. Technol. 68(10), 9604–9618 (2019)
12. Chen, J., et al.: Control of regenerative braking systems for four-wheel-independently-actuated electric vehicles. Mechatronics 50, 394–401 (2018)
13. Guo, L., et al.: Optimal energy management for HEVs in eco-driving applications using bi-level MPC. IEEE Trans. Intell. Transp. Syst. 18(8), 2153–2162 (2017)
14. Li, W., et al.: Hierarchical braking torque control of in-wheel-motor-driven electric vehicles over can. IEEE Access 6, 65189–65198 (2018)
15. Guo, H., et al.: State-of-charge-constraint-based energy management strategy of plug-in hybrid electric vehicle with bus route. Energy Convers. Manage. 199, 111972 (2019)
16. Wang, Y., et al.: Model predictive control strategy for energy optimization of series-parallel hybrid electric vehicle. J. Cleaner Prod. 199, 348–358 (2018)
17. Li, L., et al.: Model predictive control-based efficient energy recovery control strategy for regenerative braking system of hybrid electric bus. Energy Convers. Manage. 111, 299–314 (2016)
18. Zhang, J.Z., et al.: Cooperative control of regenerative braking and hydraulic braking of an electrified passenger car. Proc. Inst. Mech. Eng. Part D-J. Automobile Eng. 226(D10), 1289–1302 (2012)
19. Zhu, Y., et al.: Regenerative braking control strategy for electric vehicles based on optimization of switched reluctance generator drive system. IEEE Access 8, 76671–76682 (2020)
20. Xu, W., et al.: Velocity optimization for braking energy management of in-wheel motor electric vehicles. IEEE Access 7, 66410–66422 (2019)
21. Qiu, C., et al.: A novel control strategy of regenerative braking system for electric vehicles under safety critical driving situations. Energy 149, 329–340 (2018)
22. Lv, C., et al.: Novel control algorithm of braking energy regeneration system for an electric vehicle during safety-critical driving maneuvers. Energy Convers. Manage. 106, 520–529 (2015)
23. Zhao, X., et al.: Braking force decoupling control without pressure sensor for a novel series regenerative brake system. Proc. Inst. Mech. Eng., Part D: J. Automobile Eng. 233(7), 1750–1766 (2018)
24. Li, L., et al.: Transient switching control strategy from regenerative braking to anti-lock braking with a semi-brake-by-wire system. Veh. Syst. Dyn. 54(2), 231–257 (2016)

25. Antonov, S., et al.: Unscented Kalman filter for vehicle state estimation. Veh. Syst. Dyn. 49(9), 1497–1520 (2011)

26. Zhu, J., et al.: Braking/steering coordination control for in-wheel motor drive electric vehicles based on nonlinear model predictive control. Mech. Mach. Theory 142 (2019)

27. Cheng, S., et al.: Fusion algorithm design based on adaptive SCKF and integral correction for side-slip angle observation. IEEE Trans. Indust. Electron. 65(7), 5754–5763 (2018)

28. Song, Y.T., et al.: Direct-yaw-moment control of four-wheel-drive electrical vehicle based on lateral tyre-road forces and sideslip angle observer. IET Intel. Transport Syst. 13(2), 303–312 (2019)

29. Zhang, X., Zhu, X.: Autonomous path tracking control of intelligent electric vehicles based on lane detection and optimal preview method. Expert Syst. Appl. 121, 38–48 (2019)